# Permian Basin High Density Land Acquisition Experimental Dataset

*Stuart Farris and Rustam Akhmadiev*

## ABSTRACT

An experimental, high density land survey has been made available to the Stanford Exploration Project. Herein describes an overview of the dataset including survey parameters and employed wavelet removal techniques. Wave modes are identified in prelimanry shot gathers and possible research directions are discussed.

## INTRODUCTION

Producing oil and gas from onshore reserves has relatively low financial overhead in comparison with offshore operations (Fagan, 1997). This makes onshore production enticing during periods of oil and gas commodity recessions. Unfortunately, seismic data collected onshore is notoriously noisy and produces poor images of the subsurface. The noise and imaging issues are largely attributed to the interactions between the seismic source and the shallow-unconsolidated subsurface (Al-Ali, 2007). Better understanding the noise introduced by the shallow subsurface may lead to improved processing, modeling, and imaging of onshore oil and gas reserves.

An experimental seismic dataset was made available to the Stanford Exploration Project (SEP) through Occidental Petroleum in an attempt to better understand the surface noise within onshore seismic acquisitions. This data is particularly exciting because it a combination of 2D and 3D high density surveys. It also lies over the Delaware Basin, a subset of the Permian Basin which is a hotbed for unconventional oil and gas production in the United States. This report outlines the beginning of a long journey of processing and experimentation on this unique dataset that aims to improve the overall quality of onshore seismic imaging.

## SURVEY OVERVIEW

The acquisition parameters consist of three receiver layouts and three shot lines. The receiver geophone layouts are two patches and one line all with single phone (point receiver) recordings. The patches are square and have 441 receivers in a square 21x21 grid. They are overlain on one another and will be referred to as the 7001 patch and 8001 patch. The 7001 patch has 33x33 foot spacing and the 8001 patch has 16.5x16.5

foot spacing. The third receiver layout is a two dimensional line that extends outward from the overlain patches. This line, referred to as 6001 line, has 640 receivers spaced 16.5 feet apart. Figure 1 shows the three layouts. Figure 2 zooms in to show a closer view of the overlain patches.

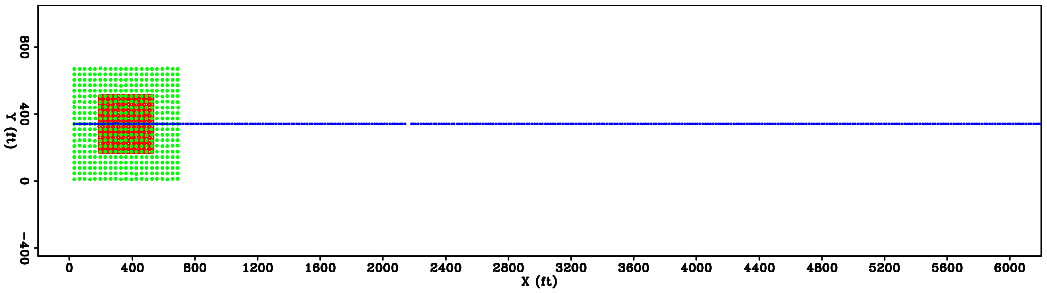


Figure 1: Receiver layouts 6001, 7001, 8001. [**CR**]

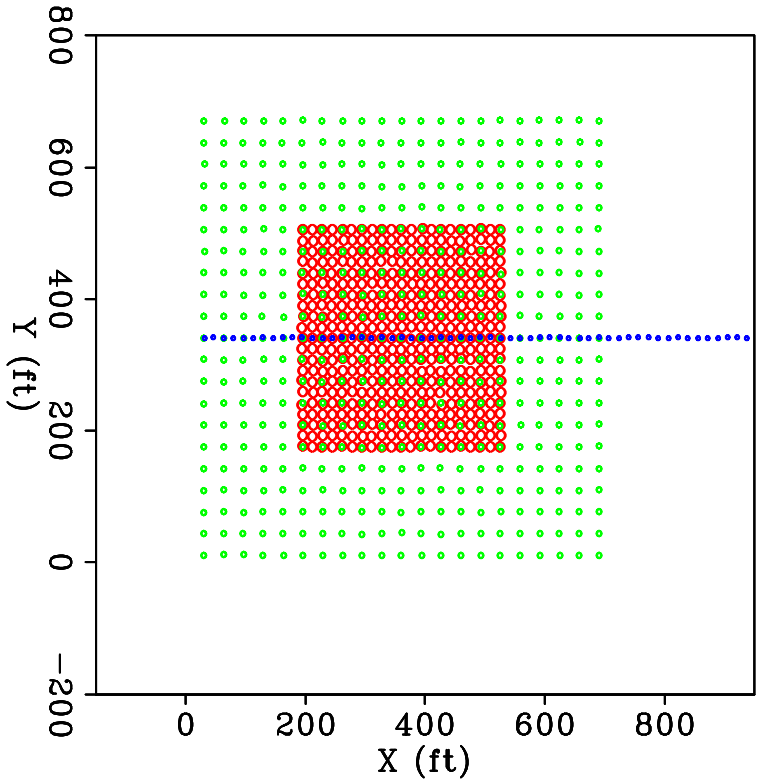


Figure 2: Zoomed view of receiver layouts 7001 and 8001. [**CR**]

Two of the shot lines extend parallel to the 6001 line with 165 foot spacing. One of the parallel shot lines lies on top of 6001 line and is referred to as the near line. The other parallel line, the far line, is offset from the 6001 line by about one mile to the north. The third shot line, the orthogonal line, runs perpendicular to the 6001 line on its western end.

Various source sweeps were used in each shot line. It is easiest to describe them in a list:

- Near Line
  - Test 1: Three sweeps per source location using four vibroseis trucks and a 16 second, 4-92 Hz linear sweep.
  - Test 2: Three sweeps per source location using one vibroseis truck and a 16 second, 4-92 Hz nominal sweep. Other three trucks were idle.
  - Test 3: Three sweeps per source location using four vibroseis trucks and a 16 second, 2-92 Hz linear sweep.
  - Test 4: Three sweeps per source location using four vibroseis trucks and a 16 second, 2-92 Hz dwell sweep.
  - Test 5: Noise test with four trucks shaking without pads in contact with ground. Performed every 16 source locations.
- Far Line
  - Test 6: Three sweeps per source location using four vibroseis trucks and a 16 second, 2-92 Hz linear sweep.
  - Test 7: Three sweeps per source location using four vibroseis trucks and a 16 second, 2-92 Hz dwell sweep.
- Orthogonal Line
  - Test 8: Three sweeps per source location using four vibroseis trucks and a 16 second, 2-92 Hz linear sweep.
  - Test 9: One sweep with one vibroseis truck every 41.25 feet using a 16 second, 2-92 Hz linear sweep.

## DATA ORGANIZATION

The previous section outlined the source and receiver geometries of this dataset. Each source pattern was used for each receiver layout. The survey has nine source patterns and three receiver layouts. This means the dataset contains $3 \times 9 = 27$ source-receiver layout combinations. We perform the wavelet removal techniques described in this report on all combinations. In this way, the quality of each technique can be assessed on a variety of source sweeps and geometries.

# WAVELET REMOVAL

Multiple wavelet removal techniques were attempted on the entire dataset with varying results. We discuss these techniques, their theoretical advantages, and their relative success. Figure 3 is included to introduce the provided raw data. From this data we hope to extract signal that represents coherent events and valuable surface noise information.

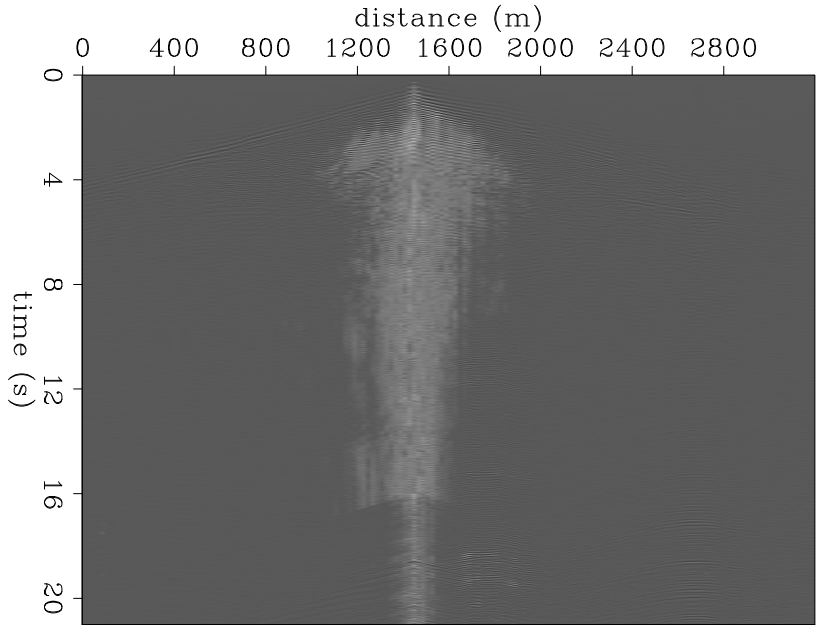


Figure 3: Uncorrelated shot gather from the two dimensional acquisition line. [**CR**]

## Correlation

The recorded vibroseis data can be represented in terms of a convolutional model, where the received signal is a convolution of the emitted source signature (sweep) and reflectivity of the earth. In frequency domain this operation corresponds to simple multiplication of their spectra. Meaning

$$\begin{aligned} d(t) &= \sum_{\tau=0}^{t} s(t-\tau) * r(\tau) \\ D(\omega) &= S(\omega) * R(\omega). \end{aligned} \tag{1}$$

Where $t$ is time, $\omega$ is angular frequency, $d(t)$ is recorded data in the time domain, $D(\omega)$ is recorded data in the frequency domain, $s(t)$ is source function in the time domain, $S(\omega)$ is source function in the frequency domain, and $R(\omega)$ is Earth's reflectivity in the frequency domain.

The most common initial step in the processing of vibroseis records is the correlation of the recorded seismic traces with the given sweep signal. This can be efficiently implemented using fast Fourier transform.

$$\begin{aligned} x(t) &= \sum_{\tau=0}^{t} s(t+\tau) * d(\tau) \\ X(\omega) &= \overline{S(\omega)} * D(\omega) = |S(\omega)|e^{-j\Phi_s(\omega)} * \underbrace{|S(\omega)|e^{j\Phi_s(\omega)}R(\omega)}_{D(\omega)} \\ X(\omega) &= \underbrace{|S(\omega)|^2}_{\text{Klauder wavelet}} * R(\omega), \end{aligned} \tag{2}$$

where $X(\omega)$ is the result of the correlation in the frequency domain. By taking the inverse Fourier transform of $X(\omega)$, we can retrieve the equivalent of the earth model convolved with a Klauder wavelet in the time domain (Yilmaz, 2001). Figure 4 illustrates the result of the correlation for the 6001 line and the 8001 patch, respectively. Since the correlation in frequency domain is periodic, the traces must be padded with array of zeros of appropriate size to avoid wraparound effect. Since the source signature is 16 seconds and the data was recorded for 21 seconds, the result of the correlation is truncated to 5 seconds.

The complex-conjugate source spectrum will have the same amplitude spectrum as the original but the phase will have the opposite sign. Therefore, cross-correlation will result into collapsing the original sweep by converting it into its zero-phase analogue (Klauder wavelet).

## Deconvolution

Another way of approaching the wavelet removal problem is solving for reflectivity directly from the correlated data found from Equation 1. However, we need to try to stabilize the solution and avoid dividing by zero. This is usually done by adding a small percent($\epsilon$) of the maximum amplitude to the denominator. We can also guarantee that the denominator is positive by multiplying the numerator and the denominator by the complex conjugate of the source spectra. Thus,

$$R(\omega) = \frac{\overline{S(\omega)}D(\omega)}{\overline{S(\omega)}S(\omega) + \epsilon A_{max}}. \tag{3}$$

The results of deconvolution are displayed in Figure 5 for the 6001 line and the 8001 patch, respectively.

## Minimum Phase Wavelet Shaping

Even when we avoid diving by zero, division itself is generally not a stable operation and can bring unwanted noise in the result. Therefore we attempt to reduce the amount of noise with Predictive Error Filter (PEF) deconvolution.

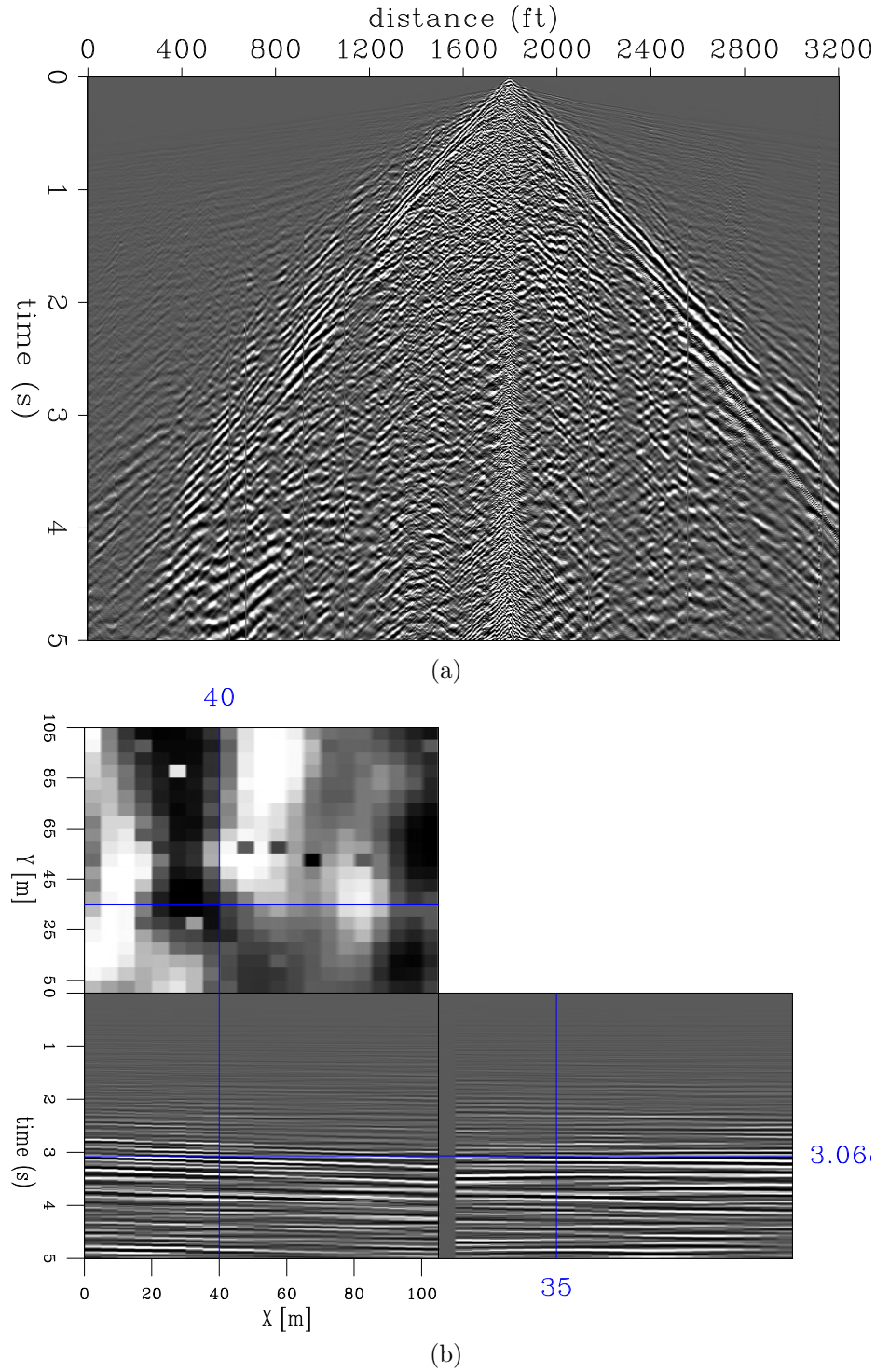


Figure 4: Correlation of shot gather from the (a) 6001 line and (b) 8001 patch. [**CR**]

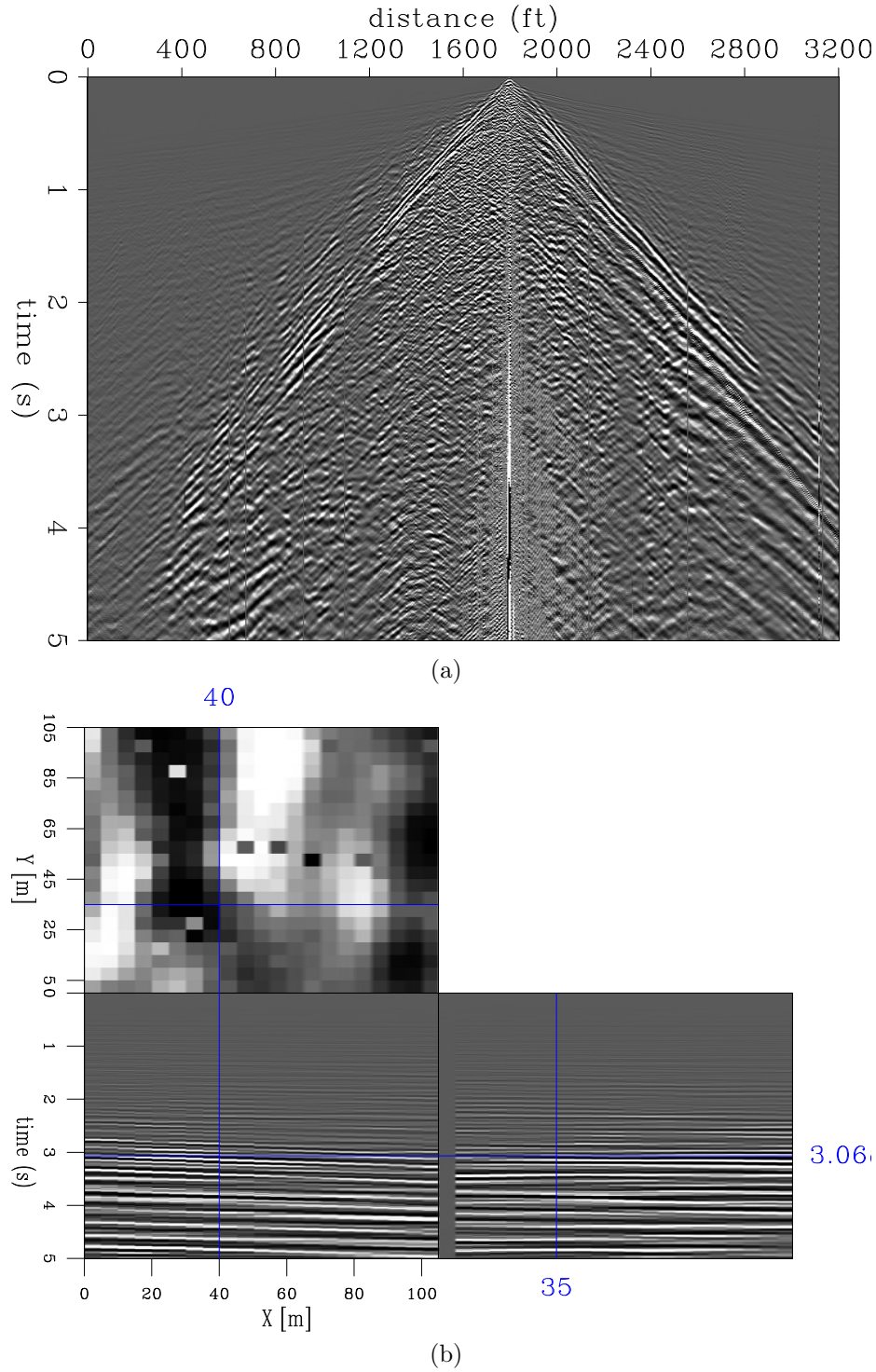


Figure 5: Decon of source wavelet from (a) 6001 line and (b) 8001 patch. [**CR**]

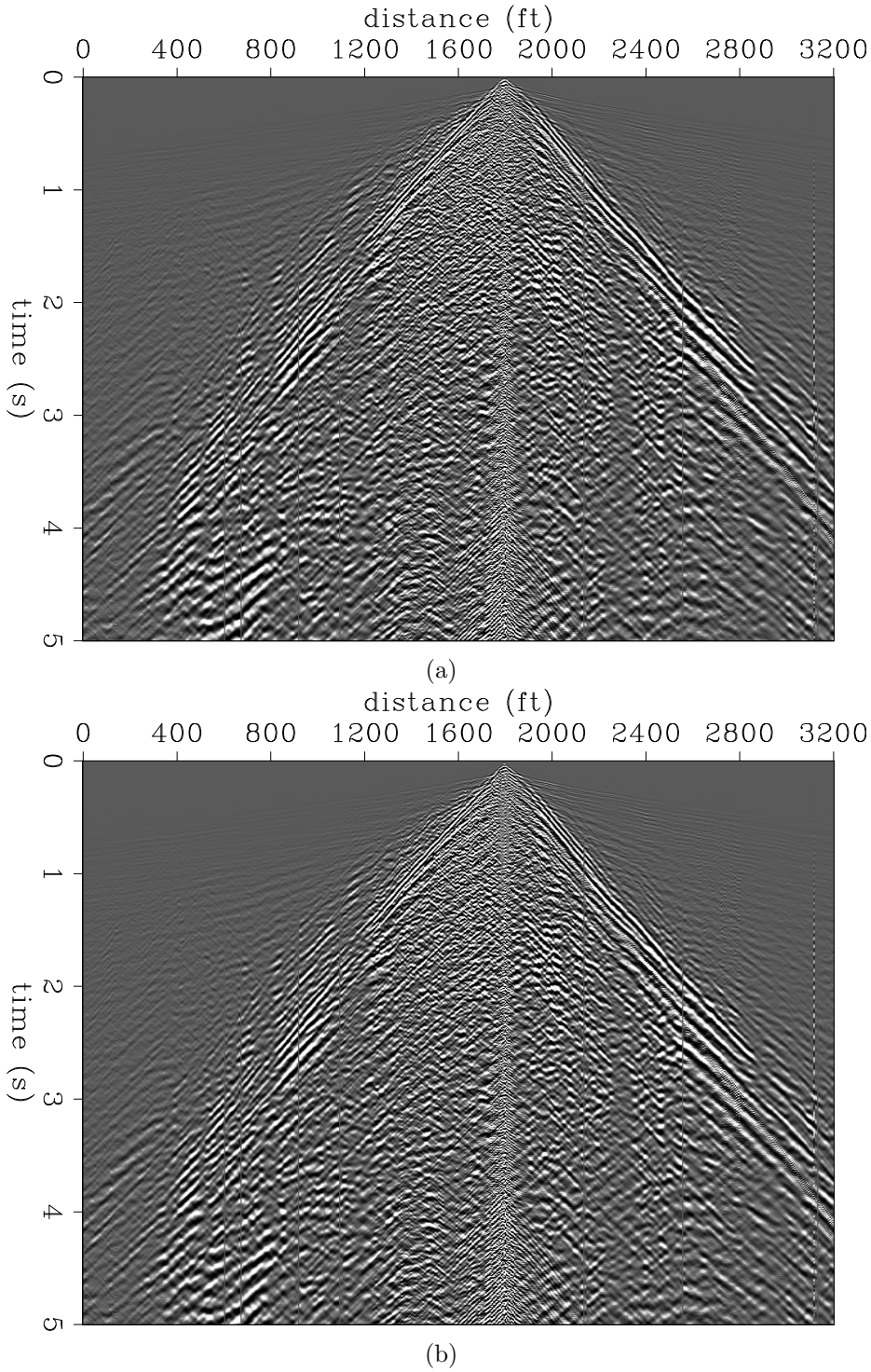


Figure 6: Correlation of shot gather from the 6001 line (a) before and (b) after min phase correction. [**CR**]

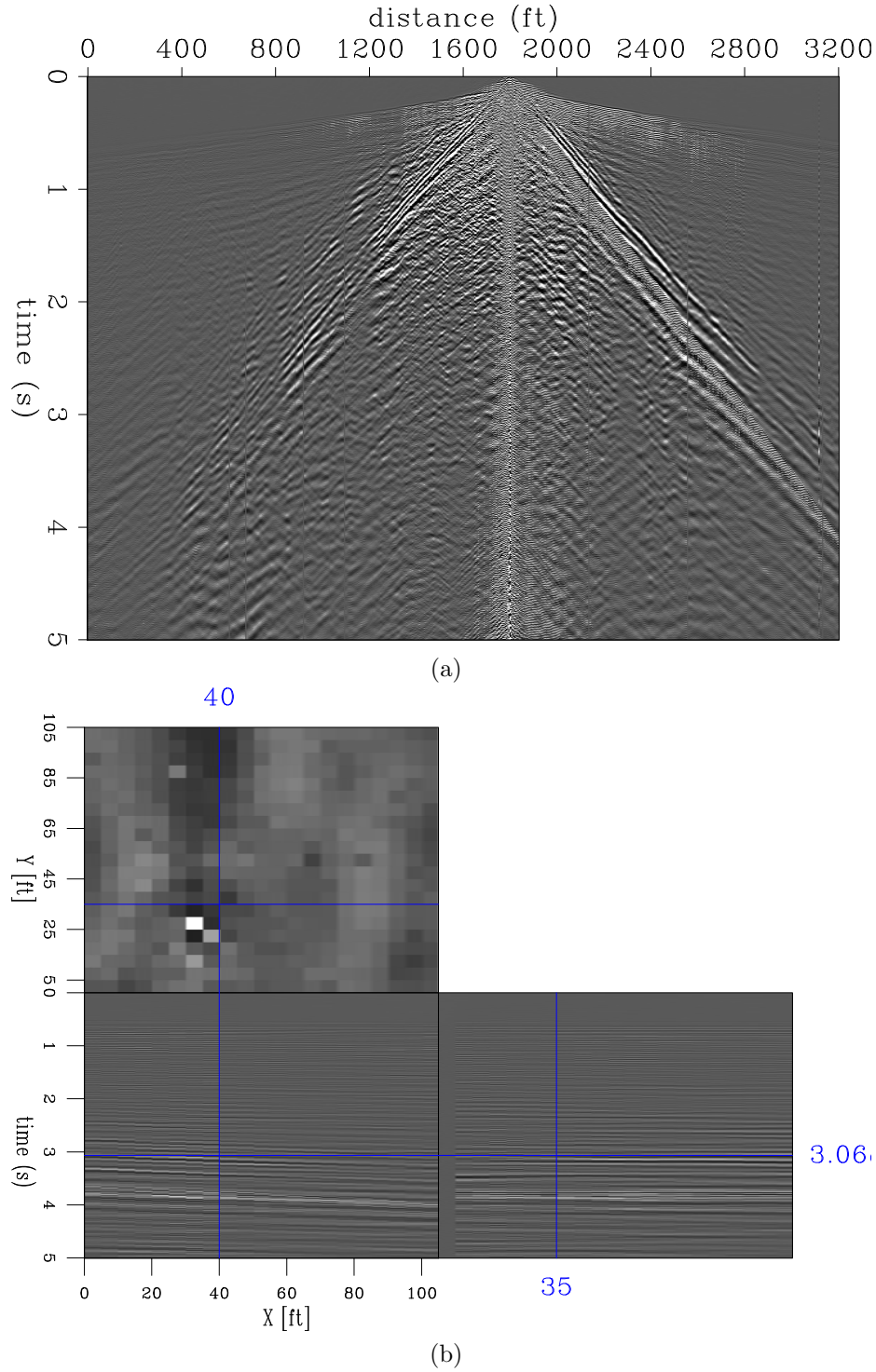


Figure 7: PEF decon from the (a) 6001 line and (b) 8001 patch. [**CR**]

However, we have seen that correlation removes the phase of the original sweep out of the record and creates a zero-phase wavelet (autocorrelation of sweep or Klauder wavelet). Strictly speaking, deconvolution is stable only for a minimum-phase wavelet, since the inverse of such a wavelet is stable and causal. That is why prior to deconvolution we need to correct the signal for the phase so that the resulting wavelet is a minimum phase analogue of the original. In order to do this Kolmogoroff factorization is used (Claerbout, 2014). This procedure creates a minimum-phase wavelet based on its spectrum, and so it can be applied to the correlated traces in order to convert the Klauder wavelet to its minimum-phase analogue.

## Prediction error filter

Using the minimum phase correction described above, PEF deconvolution can be applied to correlated traces to increase the temporal resolution of the image. In order to construct the Prediction Error Filter (PEF) of size $n+1$ and prediction interval of $\alpha$ Wiener-Hopf system of equations is solved using the Levinson-Durbin scheme (Yilmaz, 2001)

$$\begin{pmatrix} r_0 & r_1 & \cdots & r_{n-1} \\ r_1 & r_0 & \cdots & r_{n-2} \\ \vdots & \vdots & \ddots & \vdots \\ r_{n-1} & r_{n-2} & \cdots & r_0 \end{pmatrix} \begin{pmatrix} f_1 \\ f_2 \\ \vdots \\ f_n \end{pmatrix} = \begin{pmatrix} r_\alpha \\ r_{\alpha+1} \\ \vdots \\ r_{\alpha+n-1} \end{pmatrix}, \tag{4}$$

$r_i -$ is the i-th value of autocorrelation of the trace

Autocorrelation functions of the traces are averaged across all the traces in one shot gather, then the system 4 is solved for $(f_1, f_2, \cdots, f_n)$. Corresponding PEF is constructed as $(1, \underbrace{0, 0, \cdots, 0}_{\alpha-1}, -f_1, -f_2, \cdots, -f_n)$. Filter length of 50 samples and prediction gap of 1 is used. For stability, a small percent of white noise($\epsilon = 0.01$) is added to the diagonal term in the Toepplitz matrix above. The results of this PEF deconvolution are displayed in Figure 7 for the 6001 line and the 8001 patch, respectively.

Figure 8 illustrates all of the wavelet removal techniques in one plot. It can be seen that wavelet deconvolution and PEF deconvolution have brought minimal improvement to the sharpness of the recorded wavefields. Furthermore, these techniques have introduced substantial noise at near offsets and along the cone of the surface wave. Until we can improve the results of these deconvolutions, we will interpret various events using the minimum phase corrected gathers.

# WAVE MODE IDENTIFICATION

In order to get rid of the dominant linear noise present in the record, we have tried applying a FK filter to the correlated data. The following parameters for the rejection

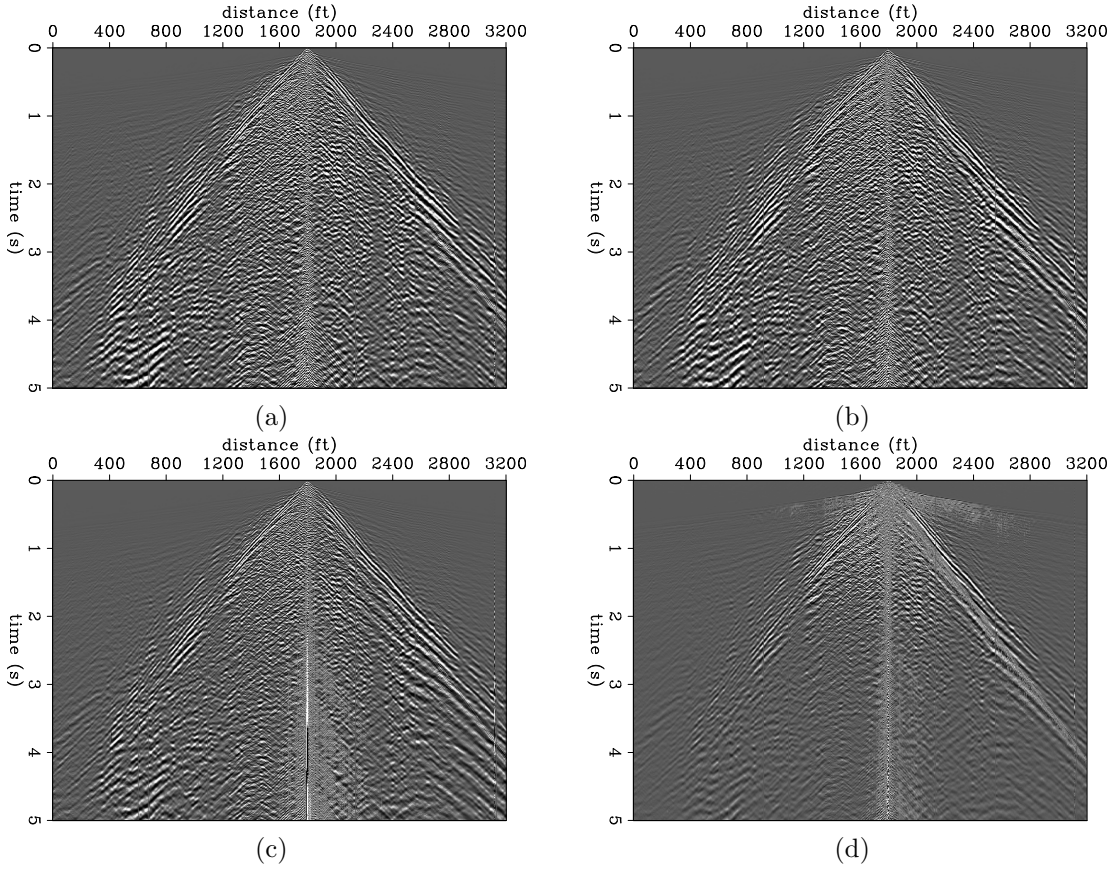


Figure 8: Shot gather from line 6001 after (a) autocorrelation, (b) autocorrelation and minimum phase correction, (c) source wavelet deconvolution, and (d) PEF deconvolution after autocorrelation and minimum phase correction. [**CR**]

zone in the FK domain were found to be suitable for surface noise removal:

- Maximum velocity - 2000 ft/s
- Minimum velocity - 0 ft/s
- Taper size - 50 samples

Figure 9 illustrates a shot with some picked events. The dominant noise in the correlated gathers is coming from the surface waves with apparent velocity of $\approx 1300 - 1400$ ft/s (shown in pink in Figures 9 and 10). There is also a fair amount of shallow back scattering shown with orange dotted lines that is characterized by a V-shaped form in the record. The first breaks are drawn as a solid red line with the velocity of refracted wave being $\approx 6000 - 6600$ ft/s. The yellow line on the figure may correspond to refracted S-wave. However, it is difficult to track and therefore this event may be coming from some other phenomena.

It is very challenging to identify reflected or diffracted waves on the record (shown in solid and dotted green lines). Nevertheless, after applying FK filter they sometimes become more apparent which allows us to pick them on the seismic gathers. These additional picks can be seen in Figure 10. However, additional work must be conducted to allow further analysis. Procedures like static corrections and median filtering may help to improve the images.

## WHAT'S NEXT

These efforts only mark the beginning of the possible investigations into this experimental dataset. There are many possible avenues for future researchers to explore. A short list includes:

1. Writing a gain program that is a function of offset.
2. Performing static corrections.
3. Performing Normal Moveout velocity analysis.
4. Comparing quality of gathers produced from linear, low frequency, and dwell sweeps.
5. Modeling surface waves.
6. Attempting full waveform inversion.

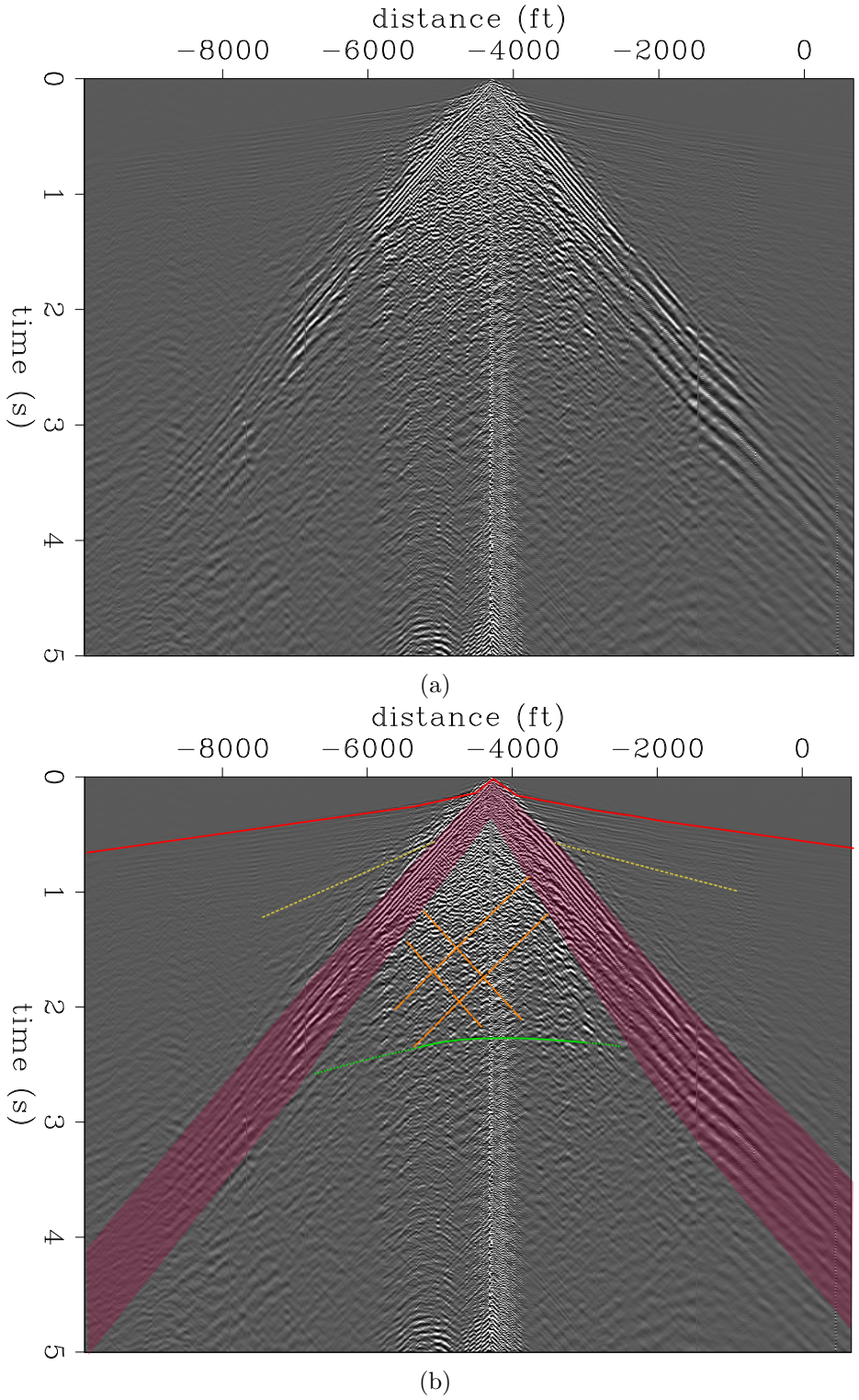


Figure 9: Identified waves in shot 33 before fk filtering: (a) without picks, and (b) with picks. [**NR**]

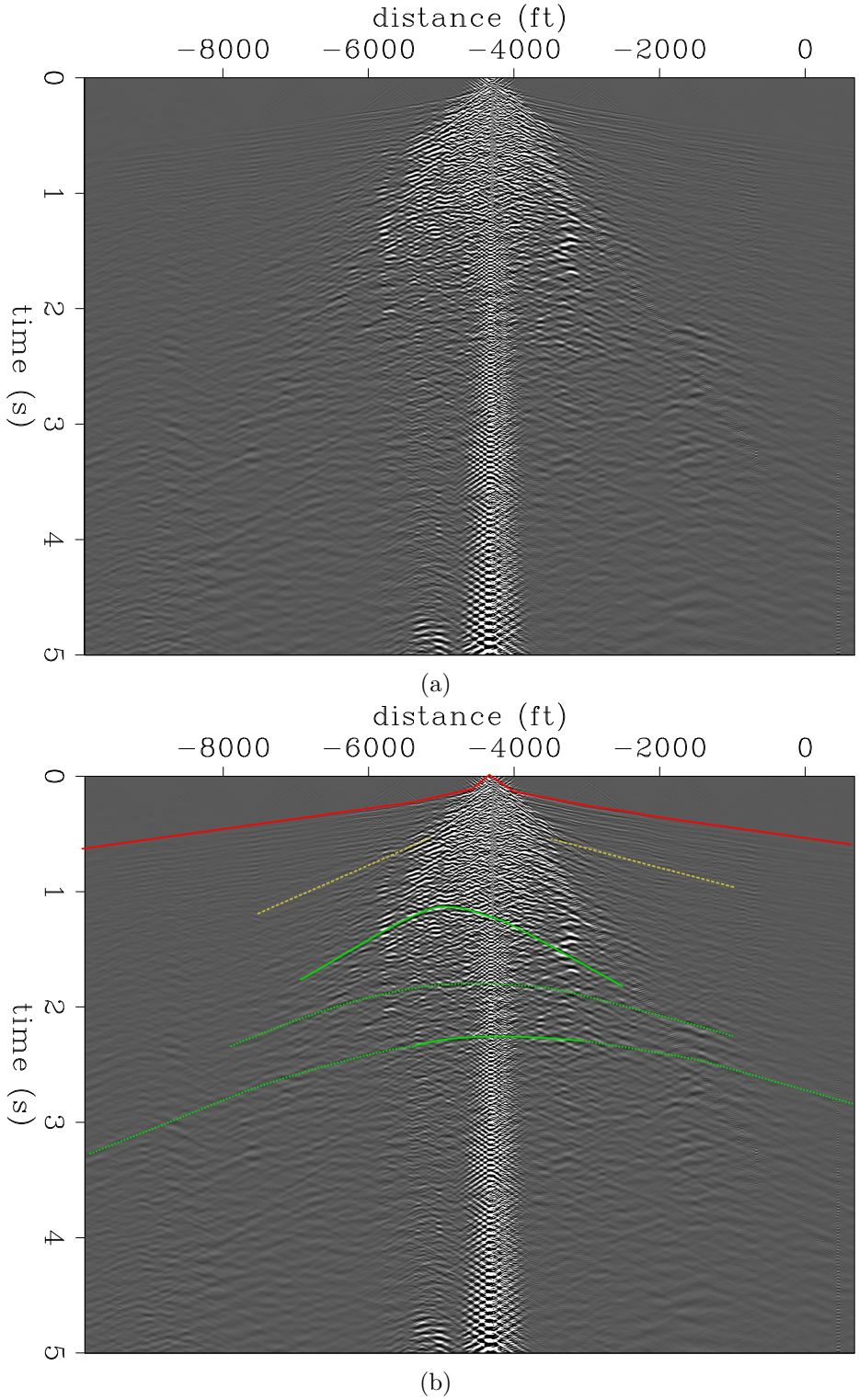


Figure 10: Identified waves in shot 33 after fk filtering: (a) without picks, and (b) with picks. [**NR**]

## ACKNOWLEDGMENTS

We would like to acknowledge Occidental Petroleum for providing the SEP with the data used in this report. A special thanks to Biondo Biondi, Shuki Ronen, Mohamed Hadidi, and Stew Levin for guidance through the messy world of onshore seismic data. Furthermore, none of this report would have been possible without Jason Chang's extensive knowledge of SEPlib and its unique 3D data manipulation. Finally, the sponsors of the SEP should be recognized for their financial support.

## REFERENCES

Al-Ali, M. N., 2007, Land seismic data acquisition and preprocessing: an operator solution to the near-surface problem: info:eu-repo/semantics/doctoralthesis.

Claerbout, J., 2014, Geophysical Image Estimation By Example.: LULU COM. (OCLC: 986953183).

Fagan, M. N., 1997, Resource Depletion and Technical Change: Effects on U.S. Crude Oil Finding Costs from 1977 to 1994: The Energy Journal, **18**, 91–105.

Yilmaz, ., 2001, Seismic Data Analysis. Investigations in Geophysics: Society of Exploration Geophysicists. (DOI: 10.1190/1.9781560801580).